A chemically inert Rashba split interface electronic structure of C_{60}, FeOEP and PTCDA on $BiAg_2$/Ag(111) substrates

2014 New J. Phys. 16 045002

(http://iopscience.iop.org/1367-2630/16/4/045002)

New Journal of Physics
The open access journal at the forefront of physics
Deutsche Physikalische Gesellschaft DPG | IOP Institute of Physics

A chemically inert Rashba split interface electronic structure of C_{60}, FeOEP and PTCDA on $BiAg_2$/Ag(111) substrates

Maren C Cottin[1], Jorge Lobo-Checa[2], Johannes Schaffert[1], Christian A Bobisch[1], Rolf Möller[1], J Enrique Ortega[2,3,4] and Andrew L Walter[4]

[1] Faculty of Physics, Center for Nanointegration Duisburg-Essen, University of Duisburg-Essen, 47048 Duisburg, Germany
[2] Centro de Física de Materiales CSIC/UPV-EHU-Materials Physics Center, Manuel Lardizábal 5, E-20018 San Sebastián, Spain
[3] Departamento Física Aplicada I, Universidad del País Vasco, E-20018 Donostia-San Sebastián, Spain
[4] Donostia International Physics Center, Manuel Lardizábal 4, E-20018 San Sebastián, Spain
E-mail: jorge.lobo@csic.es and awalter@bnl.gov

Received 31 May 2013, revised 24 February 2014
Accepted for publication 24 February 2014
Published 4 April 2014

New Journal of Physics **16** (2014) 045002

doi:10.1088/1367-2630/16/4/045002

Abstract

The fields of organic electronics and spintronics have the potential to revolutionize the electronics industry. Finding the right materials that can retain their electrical and spin properties when combined is a technological and fundamental challenge. We carry out the study of three archetypal organic molecules in intimate contact with the $BiAg_2$ surface alloy. We show that the $BiAg_2$ alloy is an especially suited substrate due to its inertness as support for molecular films, exhibiting an almost complete absence of substrate–molecular interactions. This is inferred from the persistence of a completely unaltered giant spin-orbit split surface state of the $BiAg_2$ substrate, and from the absence of significant metallic screening of charged molecular levels in the organic layer. Spin-orbit split states in $BiAg_2$ turn out to be far more robust to organic overlayers than previously thought.

Keywords: ARPES, organic electronics, spintronics, giant spin splitting, surface states, $BiAg_2$ alloy, C_{60}, FeOEP, PTCDA

In modern technological devices, organic molecules have already become important electronic building blocks due to their low cost, large variability and easy processing. For this reason, organic interfaces have become essential in all emerging electronic applications, such as spintronics. Finding suitable substrates that fit the requirements of the desired electronic device is a great challenge. Likewise, the use of molecules to their full capacities requires understanding of the interplay of the molecule–molecule and molecule–substrate interactions. In the case of organic spintronic devices, fundamental research has not yet been undertaken, particularly the investigation of organic/solid interfaces, which remain basically unexplored.

Spintronic devices are based on substrate materials with strong spin–orbit interaction. Among them, monolayer-thick surface alloys such as $PbAg_2$, $BiCu_2$ or $BiAg_2$ have received much attention since they exhibit giant Rashba splitting in their two-dimensional (2D) electronic bands. This effect is due to both: the potential gradient perpendicular to the surface direction and the sizeable in-plane potential variation caused by the different intermixed species on the surface [1, 2]. However, in order to exploit these materials in spintronic applications one needs to build up interfaces while keeping the spin texture of its bands. Inorganic magnetic films have the risk of chemically disrupting such fine surface alloys and destroying their spin properties. The alternative is the use of organic molecules, e.g. those featuring aromatic π-planes with magnetic metal cores, which generally interact more weakly with solid substrates than metallic films. The question arises as to what extent the Rashba splitting in surface alloys can be preserved upon adsorption of functional, organic molecules.

Scanning tunneling microscopy (STM) experiments in organic spintronic interfaces have already been reported, revealing the self-assembled architectures of different molecules, e.g. on the $BiAg_2$ surface alloy [3, 4]. However, the effect of the adsorption of organic molecules on the electronic structure of the $BiAg_2$ has not yet been investigated. It is the aim of this work to shed light into this matter. We therefore present the angle resolved photo emission spectroscopy (ARPES) data of three archetype organic molecules on the $BiAg_2$ surface: C_{60}, iron octaethylporphyrin (FeOEP) and 3, 4, 9, 10-perylene-tetracarboxylic acid (PTCDA). In our case, Cl–FeOEP was used to improve the stability of the molecule, however, in the following we will simple refer to it as FeOEP. In all cases, we achieve an organic/metal interface showing essentially no molecule–substrate interactions. This is manifested at both sides of the interface. In the $BiAg_2$ substrate, the Rashba-splitting in the 2D Tamm-like state persists, as in the case of physisorbed Xe [5], although in contrast to the latter, we see no modification of the energy or shape of these bands. Such a finding is quite remarkable, and will be discussed later, since such characteristics are generally attributed to topologically protected states. On the other hand, we observe a negligible metallic screening of charged molecular levels in the organic film. This effect is unusual in organic layers, which generally exhibit an upward binding energy shift from the interface to the thick film, associated with the screening of the excited hole state of the photoemission process in the proximity of the metal substrate. Therefore, the hole injection barrier (HIB) for this substrate remains almost constant from the monolayer to the thick film, which is of particular importance when envisaging electronic devices.

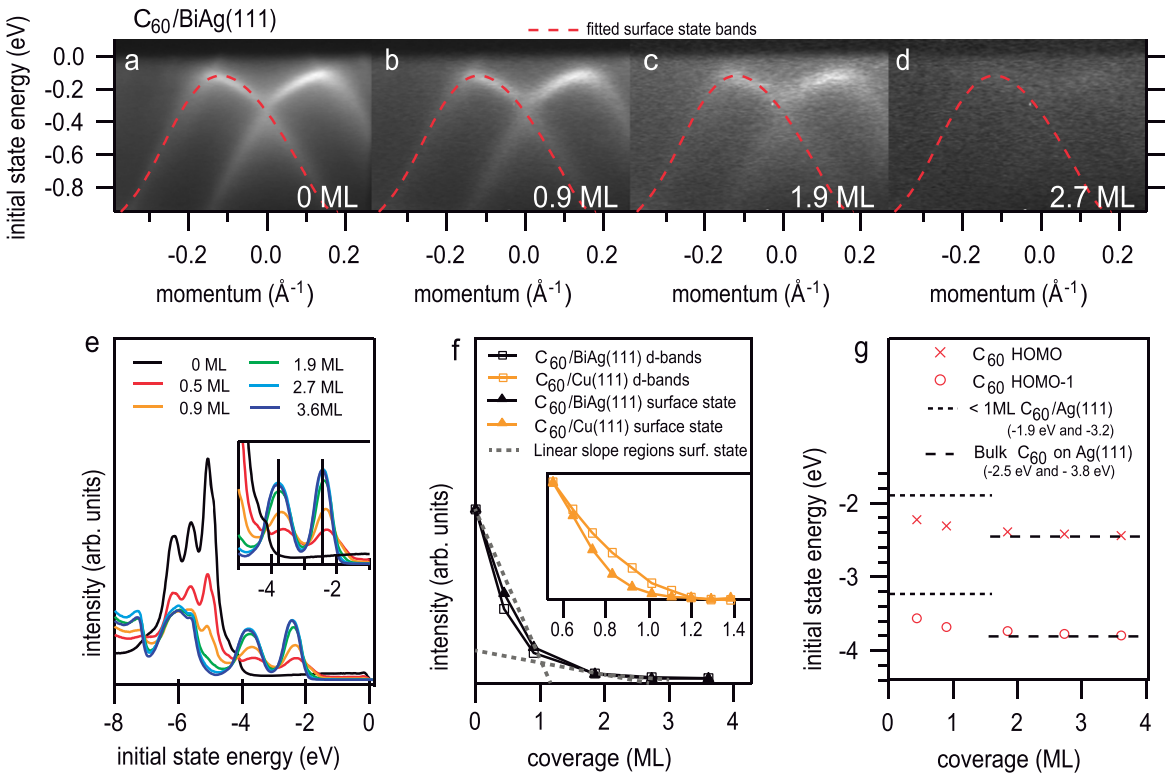

Figure 1. Experimental ARPES data from C_{60} films with different coverage on 1 ML $BiAg_2$/Ag(111). The variation in the $BiAg_2$ surface states with molecular coverage is shown in a–d, with the red dashed line a polynomial[5] fitted to the clean $BiAg_2$ surface state (used as a guide). The 0 $Å^{-1}$ intensity profiles for a range of molecular thicknesses are shown as different color lines in e. The features of the Ag d-bands are found below –4.5 eV, and new molecular orbital bands become more prominent with increasing coverage. The inset highlights the energy region above the Ag d-bands. The variation in the Ag (Cu) d-bands and the $BiAg_2$ (Cu) surface state intensity with increasing molecular film thickness is shown in f (inset to f). The intensity closely follows the gray dotted lines, indicating an almost linear decrease behavior. The variation in the position of the HOMO and HOMO-1 with molecular film thickness is presented in g and compared to that for the molecules on Ag(111) (dashed and dotted lines).

In the following, we will show and discuss the experimental ARPES data obtained from the three different molecules employed, i.e. C_{60}, FeOEP and PTCDA on the $BiAg_2$ alloy. ARPES data obtained from C_{60} films on $BiAg_2$ alloys are presented in figure 1. The effect of the C_{60} overlayers on the $BiAg_2$ surface state is shown in figures 1(a)–(d). The dashed line is a polynomial fit to the clean surface data[5] (panel a) and is used as a guide to the eye in the other panels. The most striking characteristic of this analysis is the lack of any discernable variation in the surface state, apart from a decrease in intensity with increasing C_{60} thickness. As surface states are generally significantly modified by interactions with overlayers [6–13], this suggests a very limited molecule–substrate electronic exchange.

[5] The polynomial is used to account for the s-pz and px-py hybridization of the spin-split surface states as reported by G. Bihlmayer *et al.*, PRB 75, 195414 (2007).

In all previous studies of physisorbed layers on metallic surfaces, regardless of the existence of hybridization or charge-related renormalization, a small energy shift is observed. In the case of graphene on Ir(111) [6], the surface state appears shifted toward the Fermi level by 150 meV, while the shape of the bands remains effectively unchanged. In the case of Xe absorbed on $BiAg_2$, considered an especially weakly interacting system, the bands are shifted closer to the Fermi level at the Γ-point by 50 meV and the band maxima are reduced by 20 meV. In many cases, for one monolayer of any physisorbed material on a metallic surface, the surface state is shifted toward the Fermi level by about 200 meV [6, 12, 13]. The lack of any discernable shift or modification in figures 1(a)–(d), therefore, is particularly surprising.

Normal emission (momentum = 0) energy distribution curves (EDCs) for C_{60} films with thicknesses between 0 and 3.6 ML are shown in figure 1(e). The substrate d-bands (−4.5 to −7 eV) decrease in intensity, while a number of new features (molecular energy levels) are observed to have the opposite trend. A key indication of the presence of strong molecule–substrate interactions is the formation of unique, hybridized, molecule–substrate bands at low molecular coverages [11]. Our data does not show new hybridized bands in the low coverage regions, in contrast to the clean $BiAg_2$ or bulk-like (>2.5 ML) C_{60} film, reflecting the lack of strong molecule–substrate interactions. The intensity variation of the substrate d-bands and the $BiAg_2$ surface state with coverage is shown in figure 1(f). Comparing the latter to the variation for C_{60} on Cu(111) (inset to figure 1(f)), we need higher coverages to completely suppress the d-bands and surface states in $BiAg_2$ (2 ML for the $BiAg_2$ substrate and 1.2 ML for the Cu(111) substrate). Since C_{60} on Cu(111) is already considered a weakly interacting interface that only slightly affects the surface state [8], we infer that the interaction is even weaker on $BiAg_2$, where the surface state is not quenched by the C_{60} contact layer, but its intensity is simply attenuated by the growing film. It may be argued that we have some second layer formation prior to the complete first layer being formed, such that the surface state emission belongs to $BiAg_2$ patches that remain uncovered. However, the attenuation behavior and the STM evidence for the three molecules analyzed here points against this process. As observed in figure 1(e), the decay of the Ag d-bands does not appear to be uniform. We consider this to be a consequence of the background modification and the development of molecular levels. In this case, the high binding energy peaks coincide with a conspicuous C_{60} orbital appearing when the molecule comes in contact with a noble metal [23] (energy region below 4.5 eV).

For most *in situ* grown organic films on metals, molecule–substrate interactions dominate the molecular level alignment at the interface [7–11]. In the presence of a metal, interactions range from strong chemical intermixing to weak molecule/surface interplay, with no structural disruption of the interface. However, the latter may still involve different kinds of electronic interactions, such as charge transfer and ionization, mutual polarization, or the formation of molecule/surface hybrid states [11]. All molecule/metal interactions are reflected in the energy of molecular levels, such as the highest occupied molecular orbital (HOMO), which usually evolves from the contact monolayer to the thick film. Therefore, an ideally non-interacting interface should be characterized by the absence of changes in molecular levels, which would align with respect to E_F at a constant energy from the monolayer to the thick organic film [11]. The evolution of the HOMO and the second highest occupied molecular orbital (HOMO-1) with increasing C_{60} coverage is presented in figure 1(g). For comparison, the dotted/dashed lines indicate the HOMO positions obtained for C_{60} on Ag(111) at 1 ML and bulk (>2.5 ML), respectively. The variation found in this case is much less than for the Ag(111) substrate. As a further comparison, these values, along with those for the Au(111) and Cu(111) substrates, are

Table 1. The binding energies of the two highest occupied molecular orbitals (HOMOs) for the three organic films on various metallic substrates. The underlined values are from the current measurements, while all others are literature values. All values are given in units of eV and the abbreviation n/a refers to 'not applicable'.

C_{60}	HOMO			HOMO-1		
subs.	1 ML	bulk	diff.	1 ML	bulk	diff.
BiAg2	2.31	2.44	0.13	3.68	3.80	0.12
Ag(111)	1.85 [9]	2.7 [9]	0.85	3.1 [9]	4.0 [9]	0.9
Au(111)	1.7 [14]	2.2 [14]	0.5	n/a	3.5 [14]	
Cu(111)	1.7 [8]	1.9 [8]	0.2	n/a	3.5 [8]	

FeOEP	HOMO			HOMO-1		
subs.	1 ML	bulk		1 ML	bulk	
$BiAg_2$	1.68	1.73	0.05	2.93	2.96	0.03
Cu(111)	n/a	n/a		2.69	2.89	0.2

PTCDA	$HOMO_{domain\ boundaries}$			$HOMO_{non\text{-}interacting}$		
subs.	1 ML	bulk		1 ML	bulk	
$BiAg_2$	1.63	1.76	−0.13	2.45	2.47	0.02
Ag(111)	n/a	n/a		1.55 [10]	2.45 [10]	0.9
Au(111)	n/a	n/a		1.8 [10]	2.55 [10]	0.75
Cu(111)	n/a	n/a		1.7 [10]	2.55 [10]	0.85

presented in (table 1). Note that the smallest variation between 1 ML and the bulk is observed for the current system. In a weakly interacting molecular layer, interactions with the metallic charge of the substrate realign ('renormalize' [11]) the molecular levels in the valence band spectra, which are shifted towards the Fermi energy in the organic monolayer with respect to the molecular levels of the thick films. This effect is due to both the partial metallization and hybridization of frontier orbitals in the contact organic layer, as well as to the enhanced screening of the photo-hole created in the photoemission process [11]. In reality, the charged, excited state of photoemission is the one involved in the injection processes, and hence its energy defines the actual hole injection barrier. In the case of $C_{60}/BiAg_2$, the energy shift from the monolayer to thick film ($|HOMO_{1\ ML}–HOMO_{bulk}|$) is much smaller than for the other substrates considered (~0.13 eV compared to 0.85, 0.5 and 0.2 eV for Ag, Au and Cu, respectively), and hence the HIB essentially shows no shift between one monolayer and the bulk.

The second molecule considered in the present study is FeOEP. In contrast to the case of C_{60}, FeOEP is considered a mild electron donor which features a ferromagnetic metal atom at its core. In similar systems, such a metal core has been shown to mediate strong molecule/substrate interactions [14, 15]. Therefore, we expected that the interaction with the surface may significantly increase with respect to the C_{60} case. On the contrary, the ARPES data obtained on the FeOEP covered sample, see figure 2, suggest a very similar scenario. The $BiAg_2$ surface state

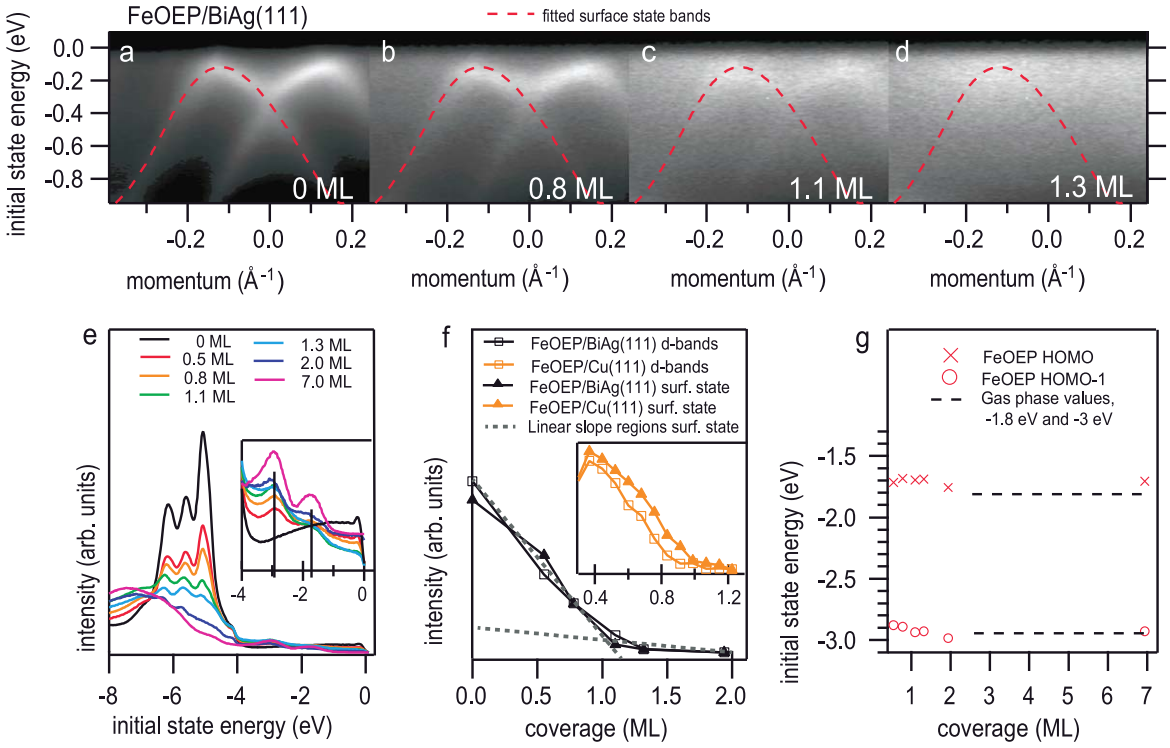

Figure 2. Experimental ARPES data from FeOEP films with different coverage on 1 ML $BiAg_2$/Ag(111). The variation in the $BiAg_2$ surface states with molecular coverage is shown in a–d, with the red dashed line a polynomial fitted to the clean $BiAg_2$ surface state (used as a guide). The 0 $Å^{-1}$ intensity profiles for a range of molecular thicknesses are shown as different color lines in e. The features of the Ag d-bands are found below −4.5 eV, and new molecular orbital bands become more prominent with increasing coverage. The inset highlights the energy region above the Ag d-bands. The variation in the Ag (Cu) d-bands and the $BiAg_2$ (Cu) surface state intensity with increasing molecular film thickness is shown in f (inset to f). The intensity closely follows the gray dotted lines, indicating an almost linear decrease behavior. The variation in the position of the HOMO and HOMO-1 with molecular film thickness is presented in g.

is again unmodified by the molecular overlayer (figures 2(a)–(d)), while the substrate d-bands and molecular orbitals show no evidence of hybridization (figure 2(e)). Also, similar to C_{60}, the evolution of the molecular level realignment from 1 ML to a thick film is minor (see figure 2(g)). We deduce that, as for C_{60} on $BiAg_2$/Ag(111), the substrate/molecular interactions are weak.

For FeOEP, the intensity of the substrate d-bands and the $BiAg_2$ surface state is attenuated more quickly with coverage, ∼1.4 ML compared to ∼2.5 ML for C_{60} (see figure 2(f)). Since d-bands are less prompted by quenching effects due to their bulk character, this difference in attenuation could reflect the mode-of-growth differences, namely island formation in C_{60} versus layer-by-layer growth in FeOEP. However, a stronger attenuation can also be explained by an effectively larger atomic density of the FeOEP film with respect to C_{60}. Nonetheless, the attenuation is still less pronounced when compared with that of FeOEP on Cu(111) (∼1.5 ML for $BiAg_2$ compared with ∼1 ML for Cu). In fact, the reasons for the peak attenuation may be more complex, since this could involve different mechanisms of electron scattering. But what is

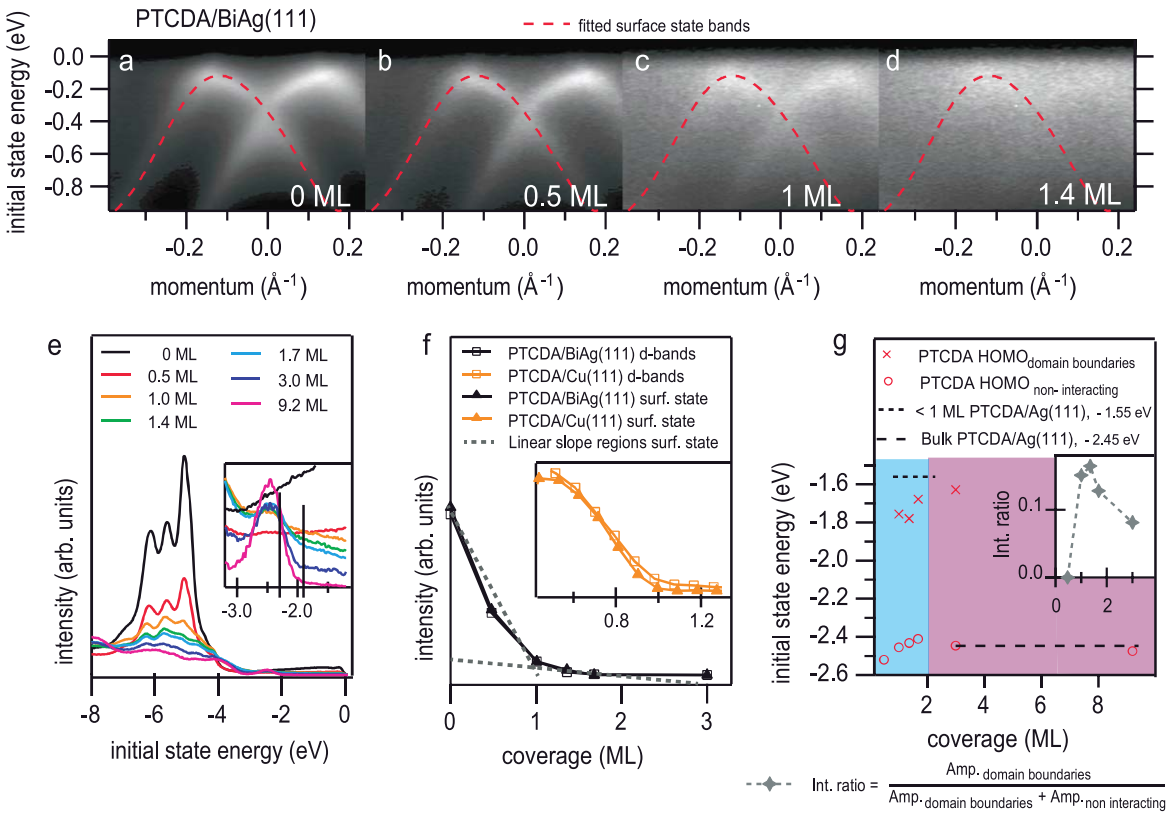

Figure 3. Experimental ARPES data from PTCDA films with different coverage on 1 ML $BiAg_2$/Ag(111). The variation in the $BiAg_2$ surface states with molecular coverage is shown in a–d, with the red dashed line a polynomial fitted to the clean $BiAg_2$ surface state (used as a guide to the eye). The 0 $Å^{-1}$ intensity profiles for a range of molecular thicknesses are shown as different color lines in e. The features of the Ag d-bands are found below −4.5 eV, and new molecular orbital bands become more prominent with increasing coverage. The inset highlights the energy region above the Ag d-bands. The variation in the Ag (Cu) d-bands and the $BiAg_2$ (Cu) surface state intensity with increasing molecular film thickness is shown in f (inset to f. The intensity closely follows the gray dotted lines, indicating an almost linear decrease behavior. The variation in the position of the HOMO derived from molecules bonded to domain boundaries and those not interacting with the substrate with molecular film thickness is presented in g and compared to that for the molecules on Ag(111) (dashed and dotted lines). The inset in g is the variation in the intensity ratio (defined in the equation below the graph) between the $HOMO_{domain\ boundaries}$ and the $HOMO_{non\text{-}interacting}$.

relevant is whether or not molecules wet the $BiAg_2$ surface. If the surface is not entirely covered at the monolayer, one could argue that the observed surface state emission corresponds to clean surface patches. As discussed below, there is significant evidence that the growth mechanism in all three molecules is layer by layer [21].

The previous two molecular films discussed, C_{60} and FeOEP, are found to barely interact with the $BiAg_2$ substrate, therefore it is interesting to also consider PTCDA, a molecule that interacts strongly with most metallic substrates [10, 11, 16, 17]. PTCDA possesses a strong acceptor character that drives a large electron transfer from the substrate, leaving the molecule in a negatively charged state. On noble metal surfaces, the PTCDA–substrate interaction varies from the strong chemisorption case of Cu(111) to the weak interaction on Au(111), passing

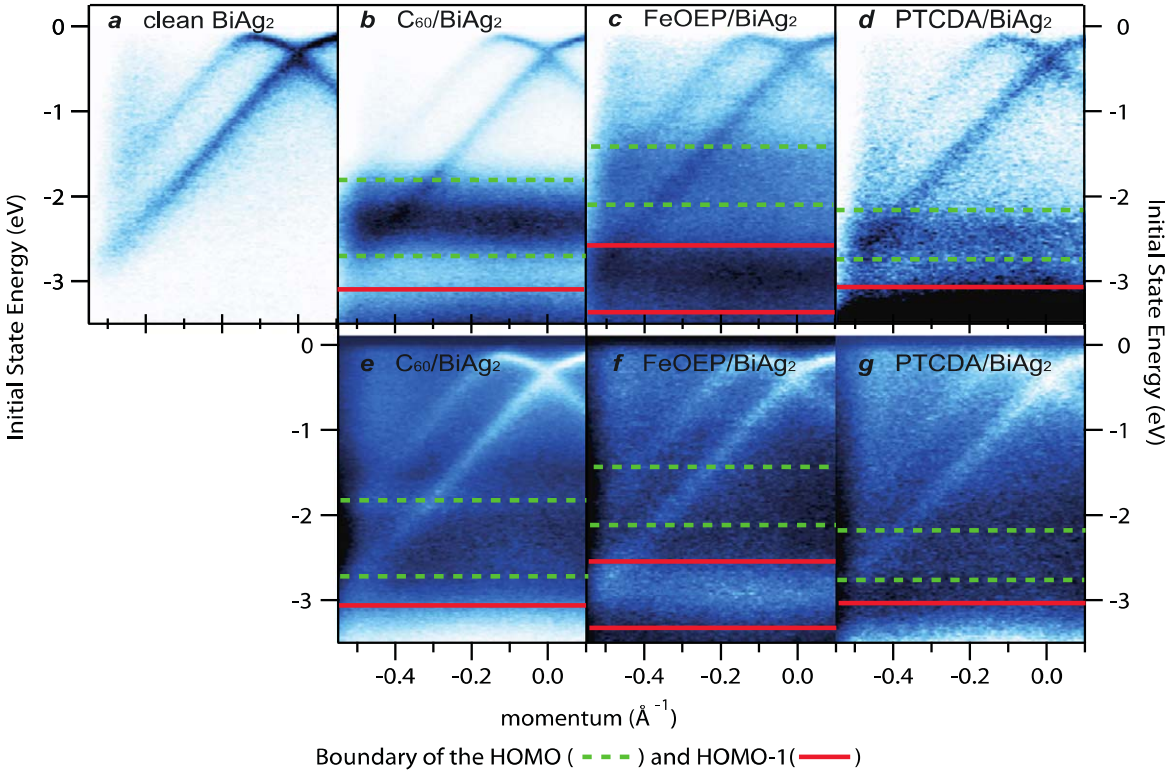

Figure 4. Detailed spectra of the $BiAg_2$ surface state for a clean sample (a), and covered with approximately one monolayer of C_{60} (b), FeOEP (c) and PTCDA (d). The same spectra as in c–d are shown in e–g after having the HOMO peak subtracted; this allows the variation in the surface state in the region of the HOMO to be investigated. The boundaries of the HOMO (dashed green lines) and HOMO-1 (solid red lines) are indicated in each case, while e–g have inverted color scales for improved visualization.

through the metallic hybrid substrate–molecule band observed in PTCDA/Ag(111) [10]. In the weakly interacting case of Au(111), the surface state lies within the HOMO–LUMO (lowest unoccupied molecular orbital) gap and shows a minor energy shift, but both the HOMO and the LUMO level still exhibit the characteristic molecular level realignment (750 meV for the HOMO and 350 meV for the LUMO [10]), i.e. an upward binding energy shift from monolayer to multilayer films [17].

Our results after depositing PTCDA on $BiAg_2$ are particularly surprising, as we again observe no significant modification with coverage of the $BiAg_2$ surface state (figures 3(a)–(d)). This undoubtedly points to an overall weak molecule–substrate interaction, which is further supported by the EDCs presented in figure 3(e). The substrate d-bands decrease in intensity with higher coverage, while the molecular levels show an opposite trend. This is similar to the C_{60} and FeOEP results presented in figures 1 and 2, respectively. The intensity variation of the substrate d-bands and the $BiAg_2$ surface state as a function of the molecular film thickness (figure 3(f)) is similar to that for C_{60} and FeOEP. Therefore, even in the case of PTCDA, which is known to interact strongly with metallic substrates, only weak substrate–molecule interactions are observed on $BiAg_2$.

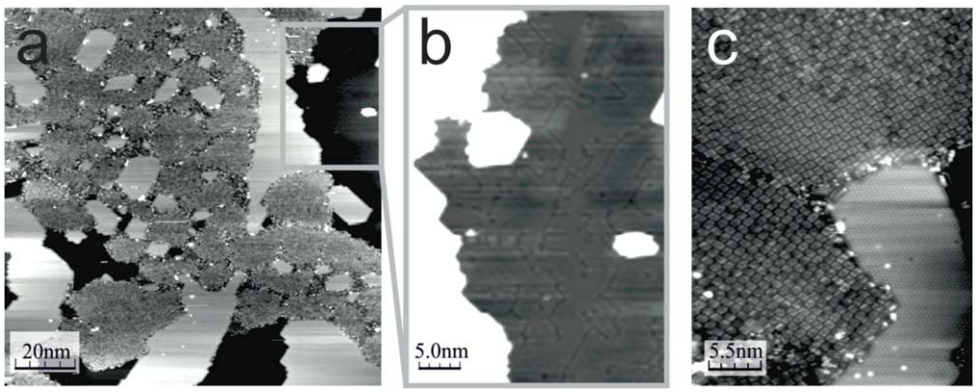

Figure 5. STM data of about 0.5 ML PTCDA on $BiAg_2$/Ag(111). The image in a shows an overview of an area close to 120 × 120 nm ($V_{sample} = 1$ V, $I_{tunnel} = 30$ pA, T = 80 K). b is a zoom into the lower area covered by $BiAg_2$, as indicated by the rectangle in a, and c shows a detailed scan of a PTCDA covered area along with an atomically resolved $BiAg_2$-island (30 × 40 nm, $V_{sample} = 1$ V, $I_{tunnel} = 100$ pA, T = 80 K).

In order to check the presence of any degree of hybridization between the molecular levels and the $BiAg_2$ surface state in any of the three different molecules, a more detailed comparative analysis of ARPES data for clean and approximately one-monolayer-covered surfaces is presented in figure 4. The surface state appears completely unchanged, except for the reduced intensity due to attenuation of the outgoing electrons in the molecular overlayer. Panels e–g in figure 4 show the equivalent photoemission data as graphs b–d after molecular orbital subtraction to rule out any possible 'hybridization effects' masked by their presence. The surface states from the substrate are observed to disperse in a completely unaffected way throughout the HOMO region, which is evidence of the lack of interaction between the molecular overlayer and the $BiAg_2$ substrate.

Coming back to the PTCDA case, due to the weak molecule–substrate interaction the alignment of the PTCDA molecular levels is expected to show a similar variation with coverage to that of C_{60} and FeOEP. However, we observe some differences that reflect the structural properties of the PTCDA monolayer, as revealed by STM. Figure 3(g) shows a shift toward E_F in the HOMO position up to about 2 ML, before it reverts into the expected inverse exponential increase in binding energy. Such behavior defines two regions (one indicated by the blue background and the second by the brown background). Figure 5 shows STM data of a $BiAg_2$/Ag(111) sample covered with about 0.5 ML PTCDA. An overview image of the sample is provided in figure 5(a). $BiAg_2$ islands are observed to form at two heights: on top, highly ordered bright regions, plus darker, shallow areas with a higher presence of defects. The PTCDA is observed to assemble within the lower, less ordered regions. In this lower $BiAg_2$ structure, a great number of domain boundaries and defects are observed (see figure 5(b)). A more detailed scan of a PTCDA-covered area can be found in figure 5(c). The lower right hand side of the image shows an atomically resolved highly ordered $BiAg_2$ island. Although the PTCDA molecules are mostly ordered within the molecular layer, most parts of the PTCDA islands show a certain disorder, which is probably induced by an interaction of the molecules with the substrate.

Molecules whose order is affected by the substrate in such a way would be expected to exhibit modified HOMO levels, and these are indeed observed in the detailed ARPES data

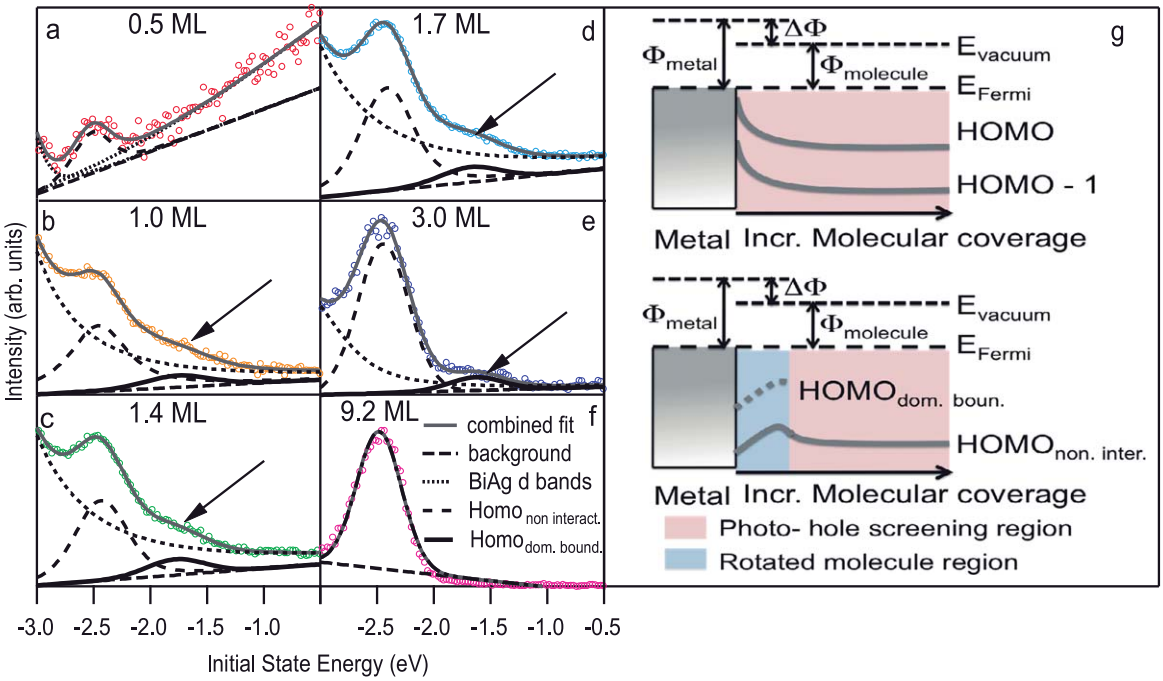

Figure 6. The results of peak fitting to the molecular orbitals for PTCDA films on 1 ML $BiAg_2$/Ag(111) from figure 3. The open circles in a–f correspond to the experimental data obtained for the different coverages. The legend for the different lines is shown in panel f. The HOMO associated with molecules at the domain boundaries (solid lines) are indicated with arrows in b to d. A schematic representation of an energy-level diagram for the case of the C_{60} and FeOEP films (top) and PTCDA films (bottom) is shown in g.

shown in figure 6(a)–(f). From our analysis, we assign one molecular feature to the HOMO of the PTCDA growing directly above the domain boundaries (black arrows). The other molecular feature at higher binding energies is assigned to the HOMO of the PTCDA growing on the 'more regular' $\sqrt{3}\times\sqrt{3}$ ordered areas. The variation in the new domain boundary HOMO is indicated in figure 3(g) by crosses. Although shifted to lower binding energy, it exhibits a similar variation to the non-interacting HOMO at low coverages. The variation in the ratio of the intensity of the two HOMO peaks (figures 3(g) inset and 6(a)–(f)) clearly indicates that this new HOMO is localized close to the substrate in the contact organic layer. Scanning tunneling spectroscopy (STS) studies have previously shown that the two rotational arrangements of the PTCDA molecules in the herringbone lattice have different molecular energy levels [11]. We interpret that at low molecular coverage, the interaction of some molecules with the substrate's domain boundaries causes significant disorder within the entire organic film, which increases the energy of the molecular levels [11]. As the molecular layer becomes thicker, the relative proportion of domain boundary interacting molecules decreases and consequently the HOMO energy changes. At sufficiently large thicknesses (>2 ML), the effect of the substrate domain boundaries is negligible and one recovers the molecular level position of the PTCDA film. In other words, the molecular level variation becomes dominated by the progressive reduction in the photo-hole screening mechanism, as observed for C_{60} and FeOEP. Energy level diagrams for the case of C_{60}, FeOEP and PTCDA are presented in figure 6(g) as a summary of the molecular alignment process in each case.

We now return to the question of the growth mode. Organic monolayers, particularly conjugated planar molecules, are known to wet metallic surfaces [21]. In the present experiment, the STM data for PTCDA indicates essentially no second layer growth at the given coverage of 0.5 ML, suggesting that the $BiAg_2$ substrate will be fully wetted before the second layer growth occurs. Therefore, we may initially discard any significant surface state emission from 'clean $BiAg_2$ substrate' patches as a way to explain the absence of surface state quenching. Moreover, layer-by-layer growth is deduced for all of our studied molecules, judging from the stepwise attenuation behavior observed in the f panels of figures 1–3 [20]. In figure 2(f) a very clear linear decrease from 0 to 1 ML is observed, followed by an abrupt change in slope and a second linear region from 1 to 2 ML. For C_{60}, the intensity decrease observed in figure 1(f) appears to have a linear region between 0 and 1 ML, followed by a second linear region with a reduced slope between 1 and 2 ML, and a third linear region, again with a reduced slope, between 2 and 3 ML. However, a lack of data points makes this assertion less strong. In figure 3(f) the same layer-by-layer attenuation behavior is again observed.

We have shown that molecular films on $BiAg_2$/Ag(111) substrates show minimal molecule–substrate interactions. The overlying molecular film does not modify the giant spin-split surface state of $BiAg_2$, and conversely the frontier molecular level energies are not modified significantly by the substrate. Therefore, both the inertness of the spintronic material ($BiAg_2$) and the organic electronic material (molecular overlayer) can be independently manipulated, and thus successfully conjugated and implemented into novel devices. The chemical inertness of the $BiAg_2$ is most striking given the metallicity of the system. Previous work has shown that metallic surface states can remain occupied under graphene layers but they are renormalized and energy shifted [6, 12, 13]. The graphene-protected Cu(111) [12] and Au(111) [13] surface states are Shockley surface states with significantly different properties to the Tamm surface state intrinsic to $BiAg_2$. The Ir(111) surface state [6] is also a Tamm state which exhibits giant spin splitting. Therefore, a similar mechanism protecting the Tamm states under both the organic film and graphene is highly likely. Varykhalov *et al* [6] suggest that the Ir(111) surface state is topologically protected, as it has tails that connect to different, occupied bulk Ir(111) bands. In contrast, no topological protection is available for the $BiAg_2$ spin-split surface state since practically all intensity is lost before reaching the higher energy, bulk Ag substrate bands. In addition, at variance with the Ir (111) surface states covered with graphene, no energy shift is observed for the $BiAg_2$ surface state. Therefore, a reduced interaction from the $BiAg_2$ surface compared with the Ir(111) surface is apparent, which accounts for the lack of energy shift in the present case.

Since topological protection must be excluded to explain the weakly interacting behavior of the organic/$BiAg_2$ interface, this should be connected to the unique chemical nature of this binary alloy. In (111), surface atoms of face-centered cubic metals are not fully co-ordinated, leaving an increased electron density at the surface which can interact with the overlying organic film. The Bi atoms, which only require three bonding partners, replace these Ag atoms in the surface layer forming the $BiAg_2$ alloy. As this arrangement results in fully co-ordinated atoms, the electron density above the surface is significantly reduced, and so is the interaction with the organic overlayers. Indeed, a similar mechanism for surface electron density reduction has been observed for $BiCu_2$ on Cu(111) [22] but was not associated with the robustness of the surface states to overlayers.

Conclusion

In conclusion, investigations of the electronic structure of C_{60}, FeOEP and PTCDA films on $BiAg_2$/Ag(111) substrates reveal that the giant spin-split surface state of the $BiAg_2$ alloy remains unexpectedly unaffected under the three molecular films. No hybridization of the substrate d-bands and molecular bands is observed, with negligible energy variations of the overlayer molecular orbitals. Such weak substrate–molecule interactions are attributed to the complete filling of electron shells in the $BiAg_2$ terminated Ag(111) surface. Remarkably, the hole injection barrier for the substrate remains almost constant throughout the studied molecular coverage. We argue that topological protection is not imposed on the system to reach the necessary chemical inertness that will electronically decouple the overlayer with the substrate. On the other hand, maintaining the substrate's spin character and the electronic nature (hole injection barrier) of the organic overlayer could create novel devices capable of manipulating each component independently, envisaging a path toward the merging of organic electronic and spintronic devices.

Methods

The ARPES experiments were conducted under UHV conditions with a base pressure better than 5×10^{-10} mbar. The measurements were performed at 150 K using the He I line (21.2 eV) from a monochromatized gas discharge lamp and a SPECS Phoibos 150 electron analyzer with energy and momentum resolutions of ~40 meV and 0.1°, respectively. In the case of the ARPES experiments, the Ag(111) sample was cleaned by repeated cycles of sputtering and annealing. One-third of a monolayer of Bi was evaporated from a well calibrated Knudsen cell while the sample was kept at room temperature. A subsequent annealing step (~550 K) ensured an alloying of the surface into one monolayer of $BiAg_2$, and low energy electron diffraction (LEED) was used to check the sample quality. Molecules were evaporated from quartz Knudsen cells while the sample was kept at room temperature. The variation in molecular thickness was obtained by evaporating further molecules onto the sample at each step. After each deposition step, the sample was checked by LEED and the respective ARPES data was collected. The molecular thickness was calibrated by comparison of wedges grown on Cu(111) to published data.

The STM experiments were conducted under UHV conditions with a base pressure better than 5×10^{-10} mbar at a temperature of 80 K. The bias voltage was applied to the sample. For data collection and processing, GXSM [18] and WSXM [19] were used, respectively. Bismuth was evaporated onto the slightly preheated Ag(111) sample from a Knudsen cell, and LEED was used to check the sample quality. PTCDA previously cleaned by gradient sublimation was evaporated from a Knudsen cell while the sample was held at room temperature.

Author contributions

This manuscript was written through the contributions of all the authors. All authors have given approval to the final version of the manuscript. ALW and MCC wrote the manuscript. MCC, JLC and ALW performed the ARPES measurements. MCC, JS, CAB and RM performed and analysed the STM measurements. ALW, MCC, JLC and JEO analyzed the data.

Funding sources

This work is supported by the Spanish Ministerio de Economia y Competitividad (MAT2010-21156-C03-01, PIB2010US-00652), by the Basque Government (IT-257-07), and the Deutsche Forschungsgemeinschaft through the SFB 616 'Energy Dissipation at Surfaces'. MCC additionally thanks the *Studienstiftung des deutschen Volkes* for support. MCC, JS, CAB and RM would like to thank the DFG for support within the program 'open access publizieren'.

References

[1] Ast C R, Henk J U, Ernst A, Moreschini L, Falub M C, Pacilé D, Bruno P, Kern K and Grioni M 2007 Giant spin splitting through surface alloying *Phys. Rev. Lett.* **98** 186807

[2] Bihlmayer G, Blügel S and Chulkov E V 2007 Enhanced Rashba spin-orbit splitting in Bi/Ag(111) and Pb/Ag(111) surface alloys from first principles *Phys. Rev.* B **75** 195414

[3] Huang H, Wong S L, Chen W and Wee A T S 2011 LT-STM studies on substrate-dependent self-assembly of small organic molecules *J. Phys. D: Appl. Phys.* **44** 464005

[4] Zhang K H L, Li H, Mao H, Huang H, Ma J, Wee A T S and Chen W 2010 Control of two-dimensional ordering of F_{16}CuPc on Bi/Ag(111): effect of interfacial interactions *J. Phys. Chem.* C **114** 11234–41

[5] Moreschini L, Bendounan A, Ast C, Reinert F, Falub M and Grioni M 2008 Effect of rare-gas adsorption on the spin-orbit split bands of a surface alloy: Xe on Ag(111)-($\sqrt{3}\times\sqrt{3}$)R30°-Bi *Phys. Rev.* B **77** 115407

[6] Varykhalov A, Marchenko D, Scholz M, Rienks E, Kim T, Bihlmayer G, Sánchez-Barriga J *et al* 2012 Ir (111) surface state with giant Rashba splitting persists under graphene in air *Phys. Rev. Lett.* **108** 066804

[7] Tzeng C T, Lo W S, Yuh J Y, Chu R Y and Tsuei K D 2000 Photoemission, near-edge x-ray-absorption spectroscopy, and low-energy electron-diffraction study of C_{60} on Au(111) surfaces *Phys. Rev.* B **61** 2263–72

[8] Tsuei K-D, Yuh J-Y, Tzeng C-T, Chu R-Y, Chung S-C and Tsang K-L 1997 Photoemission and photoabsorption study of C_{60} adsorption on Cu(111) surfaces *Phys. Rev.* B **56** 15412–20

[9] Wertheim G and Buchanan D 1994 Interfacial reaction of C_{60} with silver *Phys. Rev.* B **50** 11070–3

[10] Duhm S, Gerlach A, Salzmann I, Bröker B, Johnson R L, Schreiber F and Koch N 2008 PTCDA on Au(111), Ag(111) and Cu(111): correlation of interface charge transfer to bonding distance *Org. Elec.* **9** 111–8

[11] Koch N 2008 Energy levels at interfaces between metals and conjugated organic molecules *J. Phys.: Condens. Matter* **20** 184008

[12] Walter A L, Nie S, Bostwick A, Kim K S, Moreschini L, Chang Y J, Innocenti D *et al* 2011 Electronic structure of graphene on single-crystal copper substrates *Phys. Rev.* B **84** 195443

[13] Wofford J M, Starodub E, Walter A L, Nie S, Bostwick A, Bartelt N C, Thürmer K *et al* 2012 Extraordinary epitaxial alignment of graphene islands on Au(111) *New J. Phys.* **14** 053008

[14] de Oteyza D G, García-Lastra J M, Corso M, Doyle B P, Floreano L, Morgante A, Wakayama Y *et al* 2009 Customized electronic coupling in self-assembled donor-acceptor nanostructures *Adv. Func. Mat.* **19** 3567–73

[15] El-Sayed A, Mowbray D J, García-Lastra J M, Rogero C, Goiri E, Borghetti P, Turak A *et al* 2012 Supramolecular environment-dependent electronic properties of metal–organic interfaces *J. Phys. Chem.* C **116** 4780–5

[16] Temirov R, Soubatch S, Luican A and Tautz F S 2006 Free-electron-like dispersion in an organic monolayer film on a metal substrate *Nature* **444** 350–3

[17] Nicoara N, Román E, Gómez-Rodríguez J M, Martín-Gago J A and Méndez J 2006 Scanning tunneling and photoemission spectroscopies at the PTCDA/Au(111) interface *Org. Elec.* **7** 287–94

[18] Zahl P, Bierkandt M, Schröder St and Klust A 2003 The flexible and modern open source scanning probe microscopy software package GXSM *Rev. Sci. Instrum.* **74** 1222

[19] Horcas I, Fernandez R, Gomez-Rodriguez J M, Colchero J, Gomez-Herrero J and Baron A M 2007 WSXM: a software for scanning probe microscopy and a tool for nanotechnology *Rev. Sci. Instrum.* **78** 013705

[20] Argile C and Rhead G E 1989 Adsorbed layer and thin film growth modes monitored by Auger electron spectroscopy *Surf. Sci. Rep.* **10** 277–356

[21] Barlow S M and Raval R 2003 Complex organic molecules at metal surfaces: bonding, organisation and chirality *Surf. Sci. Rep.* **50** 201–341

[22] Bentmann H, Kuzumaki T, Bihlmayer G, Blügel S, Chulkov E V, Reinert F and Sakamoto K 2011 Spin orientation and sign of the Rashba splitting in Bi/Cu(111) *Phys. Rev.* B **84** 115426

[23] Tamai A, Seitsonen A, Baumberger F, Hengsberger M, Shen Z X, Greber T and Osterwalder J 2008 Electronic structure at the C60/metal interface: an angle-resolved photoemission and first-principles study *Phys. Rev.* B **77** 075134